Effects of dissolution conditions on the properties of PVDF ultrafiltration membranes

Title

Effects of dissolution conditions on the properties of PVDF ultrafiltration membranes

Authors

Ikechukwu A. Ike*; Jianhua Zhang, Andrew Groth, John D. Orbell; Mikel Duke

[a] Institute for Sustainability and Innovation, College of Engineering and Science, Victoria University, Melbourne, Victoria 8001, Australia.

*Corresponding author: ikechukwu.ike@live.vu.edu.au, Tel.: +61 3 99198292

Abstract

Poly (vinylidene fluoride) (PVDF) is an important membrane forming material for water treatment. Earlier works have shown that major morphological changes can be achieved when PVDF is dissolved under different conditions with practical applications in membrane distillation and protein attachment. However, no previous report has discussed the effects of dissolution conditions on the performance of PVDF under ultrafiltration, which is one of the most important applications of the polymer. In this work, four different PVDF ultrafiltration membranes were produced from dopes dissolved either by stirring at 24 °C, 90 °C, 120 °C or by sonication. It is shown that dope sonication results in membrane with enhanced thermal and mechanical stability, improved permeate flux during oil emulsion filtration and high flux recovery of ~63% after cleaning. As a comparison, flux recovery of only ~26% was obtained for the membrane produced from dope dissolved at 24 °C. The outstanding performance of the dope-sonicated membrane was linked to its slightly lower porosity, narrow distribution of small pores and relatively smooth skin layer. Performance parameters for all membranes showed good correlation to porosity suggesting a tool for membrane design achievable by simple variation in the mode of polymer dissolution. The polymer dissolution effect was related to the degree of unfolding of the polymer molecular chains and their entanglements.

Keywords

Sonication; entanglement; porosity; temperature; polymer dissolution environment; poly (vinylidene fluoride)

1. Introduction

Poly (vinylidene fluoride) (PVDF) membranes find application in a number of water treatment and separation processes and are an ongoing subject of much research due to their recognised beneficial properties such as high mechanical and thermal stability, and resistance to chemical degradation [1, 2]. There are many routes that have been developed to synthesise PVDF membranes for various applications, with non-solvent induced phase separation (NIPS) being one of the more common techniques. Several research reports have shown that the final properties of the membranes produced during a NIPS process is dependent on a number of factors such as the type of dissolving solvent, the duration of dope exposure to evaporation, and the type, temperature and impurities present in the coagulating bath [2-5]. While significant attention has been paid to properties influenced by coagulation, research is still emerging on the equally important conditions of polymer dissolution [1, 6-8]. For example, Lin et al. [7] showed that varying the temperature of dissolution of the PVDF polymer from 50 °C to 110 °C resulted in an order of magnitude change in the size of the membrane semicrystalline particles from 0.5 to 15 μm. Several other researchers have confirmed the strong effect of pre-coagulation dope preparation route on the morphological and surface properties of PVDF membranes such as porosity, crystallinity, surface energy, etc. [1, 6, 8, 9]. The lasting effect of polymer dissolution temperature has been attributed to differences in the degree of dissolution of polymer crystals in the dopes [7] as well as to differences in the extent of unfolding of the polymer molecular chains [1] prior to the membrane forming stage.

These changes to the polymer ultimately affect the practical properties of the membranes which also need to be analysed. For example, Wang et al. [1] demonstrated that the significant morphological effects arising from variations in the dissolution temperature of PVDF polymer have great impact on membrane distillation performance with flux decreasing as a result of decreasing membrane porosity as the temperature of polymer dissolution increased from 50 to 120 °C. However, the results reported by Gugliuzza and Drioli [6] for membrane produced with dopes treated to lower pre-coagulation temperatures between 30 °C and 60 °C showed increasing membrane distillation flux with increasing dope treatment temperature. Gugliuzza and Drioli related the positive effect of temperature on flux to the observed positive correlation between temperature and membrane pore sizes. The difference in the flux trends with dissolution temperature in these two reports may have resulted from

difference in the temperature range for the two sets of experiments or it may relate to the use of different solvents for phase inversion. Wang et al. [1] used water for the phase inversion of their membranes while Gugliuzza and Drioli [6] used propanol. The important point for our purpose, however, is the demonstrated strong effect of dope dissolution condition on membrane performance. Recently, Ahmad et al. [8] showed that the morphological impact and crystalline re-structuring arising from changes in the dope dissolution temperature has significant effects on the membrane protein binding ability for immunological analytical application. They showed that the protein binding properties of membranes produced from dopes dissolved above a critical temperature value of 40 °C were governed by the membrane porosity but when produced from dopes dissolved at lower temperature, the binding properties were governed by the membrane crystalline structure. Higher surface area for protein binding due to higher porosity and greater electrostatic attraction of the more polar β phase to protein were advanced to explain the results.

Although the most common applications of PVDF in membrane processes is in microfiltration (MF) and ultrafiltration (UF) [2] , there are no studies known to the authors that have evaluated the effect of polymer dissolution conditions on the properties of membranes for these two important applications. In these applications, surface hydrophilicity, pore size distribution and water flux are important as well as mechanical properties [2]. Since the proposed variation in the degree of polymer crystal dissolution and chain elongation [1, 7] are dependent on the amount of energy received during polymer dissolution, it is interesting to know how variations in energy during polymer dissolution can be utilised for designing membranes with optimal properties for MF and UF applications. It is the aim of this work to address this research need by studying the performance of PVDF UF membranes produced under four different energy environments taking particular note of the effects of the different energy environments on the membrane mechanical properties, hydrophilicity, porosity, pore size distribution and filtration performance. Three membranes were produced from dopes dissolved separately by stirring at 24 °C, 90 °C and 120 °C. The choice of the dissolution temperatures was to explore the effects over practical production temperature range. The temperatures of 90 °C and 120 °C falls well within and at the upper limit, respectively, of the common dissolution range for PVDF of 50 – 120 °C [1, 7] while the temperature of 24 °C is outside this range and also below the critical dissolution temperature of 40 °C [8]. If the environment of dope dissolution has a lasting effect on the properties of the PVDF membrane as have been advanced in the preceding discussion, high intensity radiations such as

ultrasonication may impact unique properties to the membrane [10]. Consequently, a fourth membrane was produced from dope dissolved by the novel application of ultrasonication. Although sonication has been employed routinely for the dispersion of particles in polymer solution for making membranes [11-14], it is rarely reported as a tool for polymer dissolution without the aid of mechanical stirring nor has its unique impact recognised beyond particle dispersion. This fourth method of polymer dissolution takes advantage of the highly energised environment of localised high temperature and pressure for chemical and physical changes produced as a result of the collapse of cavitation bubbles as well as other physicochemical effects arising from ultrasonication [10, 15]. All membranes were produced by the NIPS method under identical conditions except the conditions of polymer dissolution. Since every parameter and procedure were the same in the fabrication of the four membranes except the energy of the dissolution environment, it seems logical that any observed difference in the properties of the membranes can systematically be related to the effects of the different dissolution environments. To explore the effect of the dissolution conditions on the membrane properties relevant to low pressure water filtration, the membranes produced were characterised by scanning electron microscopy (SEM) for morphology, attenuated total reflectance Fourier transform infrared spectroscopy (ATR-FTIR) for crystallinity, thermal gravimetric analysis (TGA) and differential scanning calorimetry (DSC) for thermal stability and water contact angle (CA) analysis for wettability. Furthermore, mechanical strength stability and filtration performance using clean water and oil emulsion were also evaluated.

2. Materials and methods

2.1. Materials

PVDF, Solef 1015 brand from Solvay, poly(vinylpyrrolidone) (PVP), MW 40,000 g/mol, from Sigma and 1-methyl-2-pyrrilidonone (NMP) from SigmaAldrich were used for membrane fabrication. Commercial Sunflower oil and analytical grade poly (oxyethylene) (20) sorbitanmonolaurate (Tween 20) added as a surfactant were used for emulsion preparation. Elix^{TM} (type 2) water from a commercial Merck Millipore Integrated Water Purification System was used throughout this study. Elix water had a conductivity of 6.3 µS/cm and no particle was detected when analysed by the dynamic light scattering (DLS) technique using Malvern zetasizer nano ZS with size measurement range of 0.3 nm to 10 µm.

2.3. Membrane fabrication and characterisation

2.3.1. Membrane fabrication

All membranes were made by NIPS following a common procedure reported elsewhere [12, 13]. Membranes were cast from dopes prepared from 3.75 g PVDF, 0.8 g PVP and 24 g NMP and dissolved by stirring using an overhead stirrer operated at an average speed of 200 rpm at either a temperature of 24 °C, 90 °C or 120 °C and will hereafter be referred to as M24, M90 and M120 membranes. During stirring dissolution, the dopes were maintained at their respective temperature values using an oil bath set at the required temperature. The fourth dope, with the same composition as those dissolved by stirring, was prepared by ultrasonication of the polymer powders mixed in the solvent with intermittent hand mixing to move undissolved powder away from the wall of the container until the dope was clear and homogeneous. Ultrasonication usually goes on for 40 min between hand mixing. A probe-type sonicator (Hielscher Ultrasonic Processor UP400S) operated at an effective power of ~10 W, sonic irradiation pulsing of 30% and a working frequency of 24 kHz was used. During ultrasonication, the dope, contained in a 100 ml glass beaker, was cooled by an oil bath immersed in an ice bath to reduce the possibility of water contamination. The dope average temperature during ultrasonication resulting from the conversion of the dissipated sonic energy to heat energy was ~ 110 °C. The average temperature of the ultrasonication environment was defined by the ultrasonication conditions and the efficiency of the cooling system. The membrane made from the sonicated dope will hereafter be referred to simply as Sonic. After complete PVDF dissolution, which was assessed visually by noting when the dope was wholly homogeneous and clear, each dope was allowed to stand for at least 1 h to equilibrate with the ambient condition. Typically, complete PVDF dissolution was achieved between 2 to 3 h for M90, M120 and Sonic while 8 h or more were needed for M24. Similar dependence of PVDF dissolution time on the energy of dope dissolution environment has been previously reported [1, 7]. The dopes were not maintained at their dissolution environment for the same length of time (>8 h) because increasing ultrasonication time well beyond 3 h significantly impaired the Sonic membrane properties while the other membranes were not affected. This informed the decision to standardise the dope by ending dissolution once the dope was visually clear and homogeneous. Previous works have demonstrated that the specific effects of variable temperature dissolution environments are observed when dopes were maintained for the same extended duration in different dissolution environments [1, 8] or when they were subjected to dissimilar dissolution times [7]. Ahmad et al. [8]

specifically reported that PVDF membrane properties were independent of practical dissolution time but dependent on dissolution environment. After clear polymer solutions have equilibrated to room temperature conditions, they were hand cast on glass plates using an Elcometer adjustable doctor blade set to a nominal opening of 300 µm before phase inversion in room temperature Elix water. The membranes were placed in the Elix water for at least 24 h at room temperature and subsequently were stored wet at 4 °C.

2.3.2. Membrane characterisation

Samples for SEM, ATR-FTIR spectroscopy, TGA and DSC, CA analysis and mechanical strength tests were dried at room temperature prior to analysis while wet membranes were used for other characterisations. Surface SEM images were acquired on a Zeiss Supra 55VP FEG SEM. Cross section SEMs were acquired using a FEI Quanta 3D FEG Scanning Electron Microscope - gallium dual beam. The membrane cross sectioning was made by ion milling. Milling with the Gallium Focus Ion Beam (Ga FIB-SEM) was performed at 20 keV and in three steps, including a rough milling step at 3 nA and two cleaning steps at 1 nA and 0.3 nA. To determine the average size of the pores on the selective surfaces of the membranes, the SEM images of the membrane skin layers were processed using ImageJ (https://imagej.nih.gov/ij/). ATR-FTIR was used to study the crystalline phase of the PVDF membranes. The crystalline mass fraction of the β-phase was computed using Equation 1 [16]

$$F(\beta) = \frac{P_\beta}{1.26P_\alpha + P_\beta} \qquad 1$$

where $F(\beta)$ is the mass fraction of the β phase in a sample of PVDF polymer and P_α and P_β are absorption peaks of the α and β phases corresponding to the characteristics wavenumbers of 763 and 840 cm^{-1} respectively. TGA and DSC studies were simultaneously conducted using a Mettler Toledo Thermal Analyser TGA/DSC 1 STAR^e system under nitrogen flow of 20 mL/min and steady temperature increment of 10 °C/min until a temperature of 700 °C was reached. Membrane water CA was measured using an Attension Theta Optical Tensiometer operated at room temperature. The bulk porosity, ε, for each membrane was computed gravimetrically by first measuring the mass of a membrane piece wet with water [17, 18]. Loose water on the membrane surface was wiped off with paper towel before weighing [8]. The membrane piece was then dried in an oven at 60 °C for at least 24 h and was re-weighed subsequently. Porosity was computed using the following equations [8, 17, 18]:

$$\varepsilon = \frac{(M_w - M_d)/\rho_w}{(M_w - M_d)/\rho_w + {}^{M_d}/_{\rho_P}} \quad (2)$$

where M_w is the mass of the wet piece of membrane, M_d is the mass of the dry piece of membrane, ρ_P and ρ_w are the density of PVDF (1.78 g/cm^3) and water (1 g/cm^3), respectively [8]. Mechanical strength tests were conducted using an Instron Materials Testing Instrument, with a 5 kN load cell. Dry samples were cut into 10 cm x 1 cm strips for mechanical strength test conducted by sample extension at a constant speed of 10 cm/min at room temperature [12, 17]. A shrinkage test was performed to better understand the mechanical strength properties of the dry membranes. The shrinkage test involved measuring the area of a piece of membrane when wet (A_w) and after drying (A_d) at room temperature. Observed reduction in membrane thickness was negligible compared to contraction in area. Consequently, the shrinkage (S) was defined as the percentage reduction in membrane area due to drying:

$$S = \frac{A_w - A_d}{A_w} \times 100 \quad (3)$$

2.3.3. Filtration experiments

Fresh oil-in-water emulsions were produced for filtration experiments by homogenising 1.5 g sunflower oil and 0.5 g Tween 20 in 1 L Elix water using a Unidrive X 1000 homogeniser operated at 17,500 rpm for 30 min. The droplet size distribution of the resulting white emulsion was characterized by the DLS technique using a Malvern zetasizer nano ZS. The emulsion remained stable for several days with no change in the milky appearance and thus suitable for membrane tests conducted over a period of a few hours each. The filtration experiment involved the measurement of three sequential fluxes on wet membranes: membrane clean water flux (J_0) determined from 30 min of water filtration; emulsion flux (J_1) obtained from 2 h emulsion filtration; and membrane after-fouling clean water flux (J_2) determined from 30 min of water filtration after emulsion fouling and membrane cleaning. The J_2 flux measurements were preceded by 20 min of water filtration to remove foulant cake; a 30 min chemical flush using 0.1 M NaOH solution as a mild cleaning agent; and another 20 min of water filtration to rinse the NaOH solution. The average membrane flux recovery, (*FR)* defined as [13]:

$$FR(\%) = \frac{J_2}{J_0} \times 100 \quad (4)$$

was computed for each membrane using average clean water flux values J_0 and J_2. Each series of flux measurements for a clean membrane were preceded by an initial membrane compaction by water filtration at 50 kPa transmembrane pressure (TMP) for 30 min. Flux measurements were conducted under a constant TMP of 30 kPa and cross flow velocity of 13 cm/s (volumetric flow rate of 10 cm^3/s) using a crossflow acrylic module from Sterlitech®. Figure 1 is the schematic of the filtration setup. The permeate mass was constantly measured over a balance and logged to a computer every minute. The feed and permeate total carbon (TC) were measured using a Shimadzu TOC-V_{CSH} Total Organic Carbon Analyzer. These values were used in evaluating the membrane rejection (*R)* computed using the expression:

$$R(\%) = \left(1 - C_p/C_f\right) \times 100 \qquad 5$$

where C_p and C_f denote permeate and feed TC concentrations (mg/L), respectively.

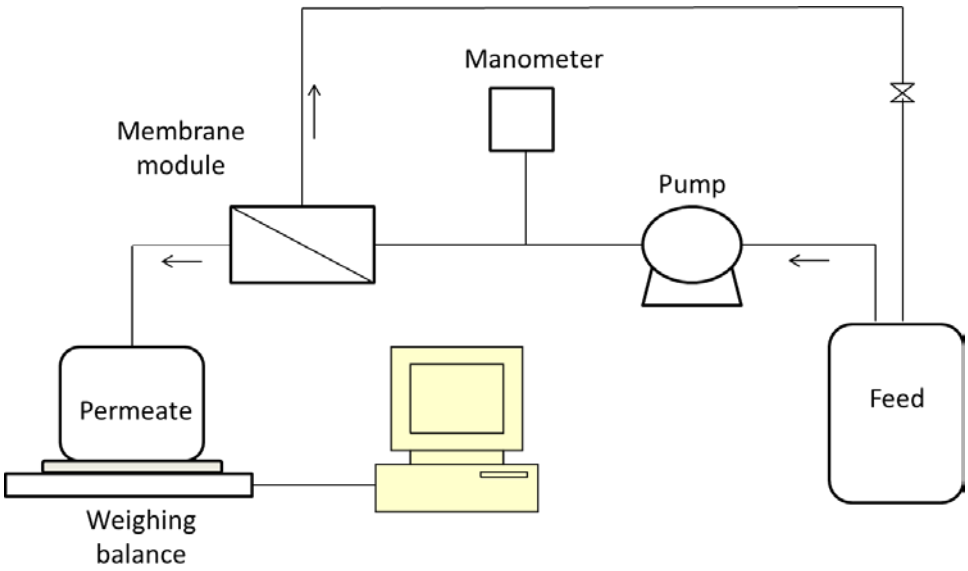

Figure 1. Schematic diagram of filtration set up

3. Results and discussions

3.1. Membrane morphology

The morphological features of the membranes were examined by SEM. Figure 2 is the skin layer and cross section images of the membranes.

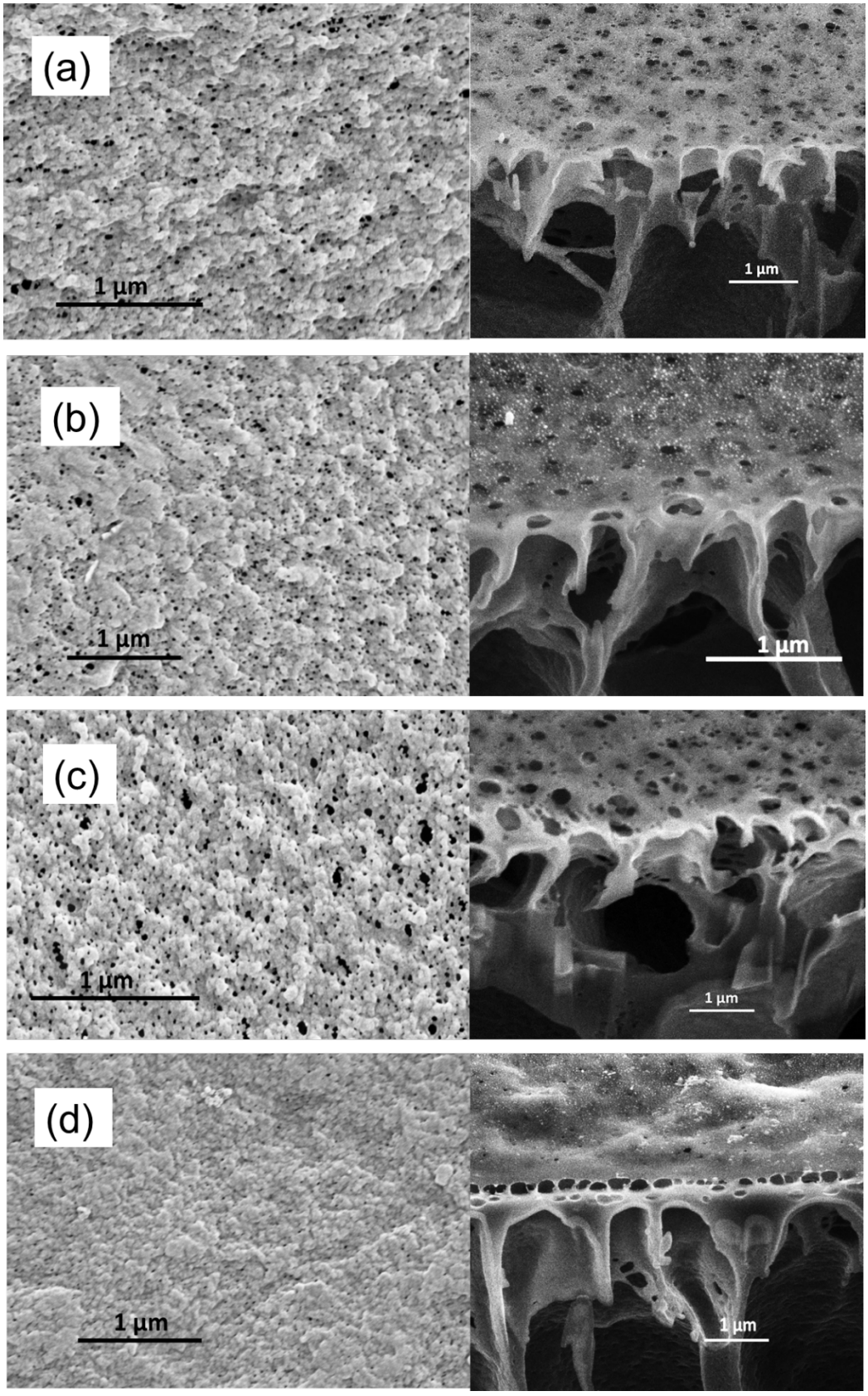

Figure 2. SEM images of membrane skin layer (left) and cross section (right) for M24 (a) M90 (b) M120 (c) and Sonic (d).

The membrane cross sections clearly shows typical asymmetric structural features characteristic of phase inversion in a strong non-solvent such as water with a thin selective skin layer of relatively smaller pore sizes resting on larger macrovoids [2]. Relative to Sonic, the membrane skin layer surface and cross sections for M24, M90 and M120 appeared reasonably similar, with a rough and nodular appearance. The roughness appears to develop from scattered and irregular depressions in which most of the membrane pores are formed. This unique structural arrangement seems to create the impression of very large skin layer pores in the cross section images. However, some of the impressions of large pores observed in the cross sections especially those closer to the line of ion milling may be real and are believed to have developed from stray ion beam during ion milling. Uniquely, the M120 showed slightly larger pore openings compared to M24 and M90. Figure 2 shows that Sonic is markedly different from the other membranes. Its relatively smooth surface and lack of apparent pore openings at the resolution of the figure are contrasted by the roughness and large pores of the other three membranes made without sonication. In addition, the relatively dense skin layer resting on slightly more ordered macrovoids of the Sonic creates the impression of a sturdy membrane framework and further distinguishes it from the other membranes.

3.2. Crystalline phase

Typical FTIR spectra for the membranes are shown in the Supplementary Material (Figure S.1). The similarity of the spectra is an indication that physical differences in the membranes cannot be explained by chemical changes during the various polymer dissolution processes. The computed $F(\beta)$ using Equation 1 based on FTIR data is given in Figure 3. It is evident that $F(\beta)$ increased steadily with the dissolution temperature of the polymer. PVDF has been reported to crystallise in at least four different polymorphs under various conditions [1, 2, 19]. The most common polymorphs are the α and β phases. The β phase has been associated with a number of interesting properties such as piezo-, pyro- and ferroelectric effects and has also been connected with enhanced mechanical strength of the polymer [16, 20, 21]. The all *trans* conformation of the polar β phase are known to be favoured when PVDF is crystallised from solution while the *trans-gauche trans-gauche* conformation of the non-polar α phase are known to crystallise readily from the melt [19, 22]. The maximum $F(\beta)$ of 68% was recorded for M120 while the Sonic followed closely with a mass fraction of 66%. The lowest $F(\beta)$ of

56% was computed for M24 suggesting strong dependence of crystal phase on temperature of dope dissolution.

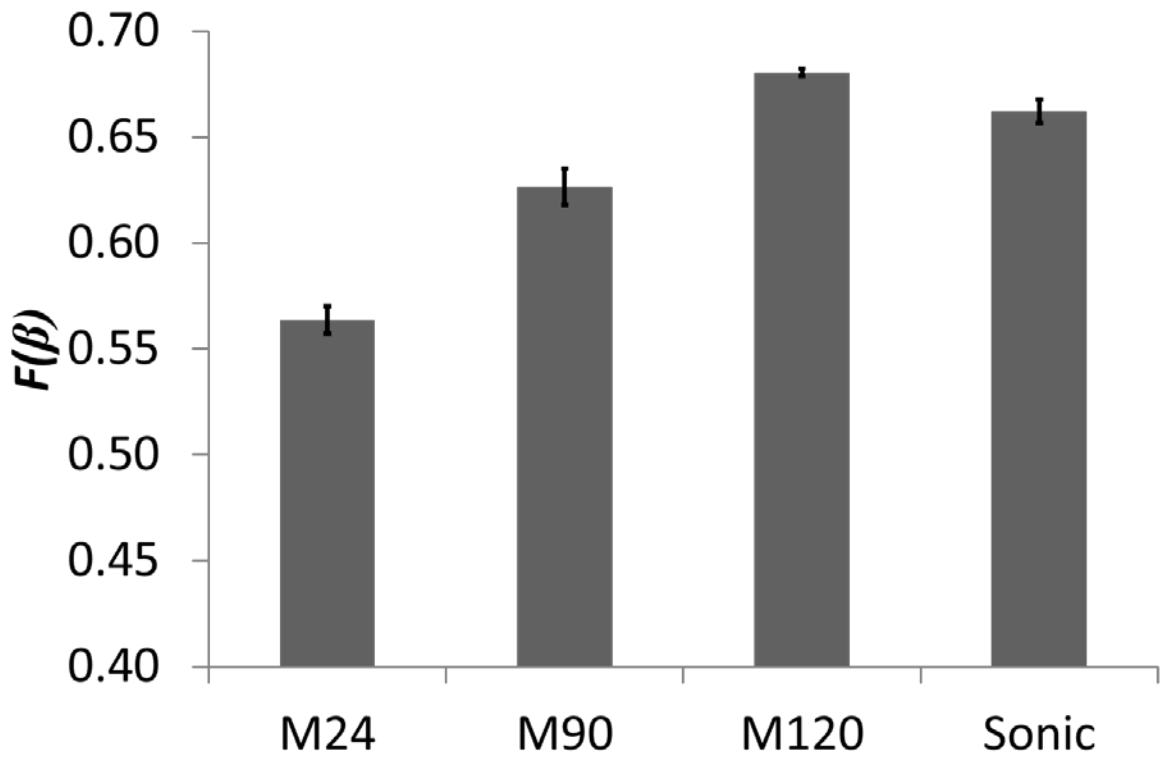

Figure 3. Membranes β-phase mass fractions, *F(β)*, from FTIR data using equation 2. Error bars indicate computed standard error.

Ahmad et al. [8] documented significant influence of dissolution temperature on the crystallinity of PVDF membranes as measured by FTIR. However, in their work, the *β* phase was reported to decrease with temperature of dope dissolution from a value of ~70% at 20 °C to ~45% at 100 °C. This is a reversal to the trend observed in this work. The divergence in trend may be linked to differences in coagulating solvent. Ahmad et al [8] used 2-propanol (a soft non-solvent) as their coagulating solvent while water (a harsh non-solvent) [2] was used in this work. Since the *β* phase is the polar form of PVDF [19], the polarity of the coagulating solvent might influence the crystalline structure of the polymer during the phase inversion process. However, Lai et al [12] reported a low *β* phase of only 17% for PVDF membrane produced by stirring at 90 °C with phase inversion in 60 °C deionised water. Furthermore, Wang et al. [1] and Lin et al. [7] reported that the temperature of dope dissolution had no effect on membrane crystalline phase with only the α phase of PVDF identified. It is worthy

of note that these last two groups assessed crystalline phase by the X-ray diffraction (XRD) method. It appears that the XRD technique is a less sensitive method for characterising PVDF crystalline phases probably due to the limited crystallinity of PVDF. XRD is more suitable for characterising long range order crystallinity since it averages the properties of materials over the entire structure while FTIR probe material properties over a short range [23, 24]. Lekgoathi and Kock [24] recently showed that Raman spectroscopy was more sensitive than XRD analysis in characterising the short range order crystalline structure of $LiPF_6$. Since Raman scattering is a vibrational spectroscopic technique like FTIR, the report by Lekgoathi and Kock [24] supports the proposal that FTIR is probably more sensitive than XRD in characterising PVDF crystalline phases.

3.3. Thermal stability

The results of the DSC and TGA performed on the membranes are given in Figure 4. The DSC results shows that the four membranes have similar glass transition temperature (T_g) of about 36 °C which is close to the PVDF literature value of 40 °C [25] as well as similar melting point (T_m) of 172 °C which closely matches both the PVDF supplier data and literature values [25, 26]. These results indicate that the pre-melt properties of the membranes, namely, chain alignment and crystallinity [25], were practically unchanged by the dope dissolution techniques. Ahmad et al. [8] also reported unchanged pre-melt thermal properties for PVDF membranes produced from dopes dissolved by stirring under different temperature conditions between 20 °C and 100 °C despite significant morphological differences between the membranes. However, it can be seen in the TGA results that the initial onset of thermal degradation (T_d), defined as the temperature at 1.5 % thermally induced weight loss [27], was significantly influenced by the polymer dissolution conditions. Sonic showed the highest T_d of about 350 °C. Decomposition temperatures for M24, M90 and M120 were 300 °C, 340 °C, and 315 °C respectively. The minimum T_d for pure PVDF has been given as approx. 330 °C [25]. The T_d values reported in this work are similar to the T_d of 320 °C reported by Zhang et al. [27] for PVDF membrane with incorporated PVP (for hydrophilicity enhancement) as was the case in this work. The TGA results in this work indicate that while sonication improved thermal stability, low temperature (24 °C) and high temperature (120 °C) dissolution conditions impaired membrane thermal stability. Improvement in resistance to thermal decomposition has been associated with higher molecular weight and more cross linking due to reduced number of end groups and restrained

molecular movement [25]. Reduction in the number of end groups and restrained molecular movement may also develop from higher degree of polymer chain entanglement in the melt [28, 29] resulting from high energy dissolution environments [1, 7] thus increasing the polymer T_d. This proposal may explain the higher T_d for Sonic and M90 and the lower value for M24. The lower T_d for M120 may suggest the initiation of some degree of polymer chain scission [25] at the dissolution temperature of 120 °C which reduced chain entanglement and consequently T_d. Structurally weak PVDF membrane at higher dissolution temperature have been previously reported [7].

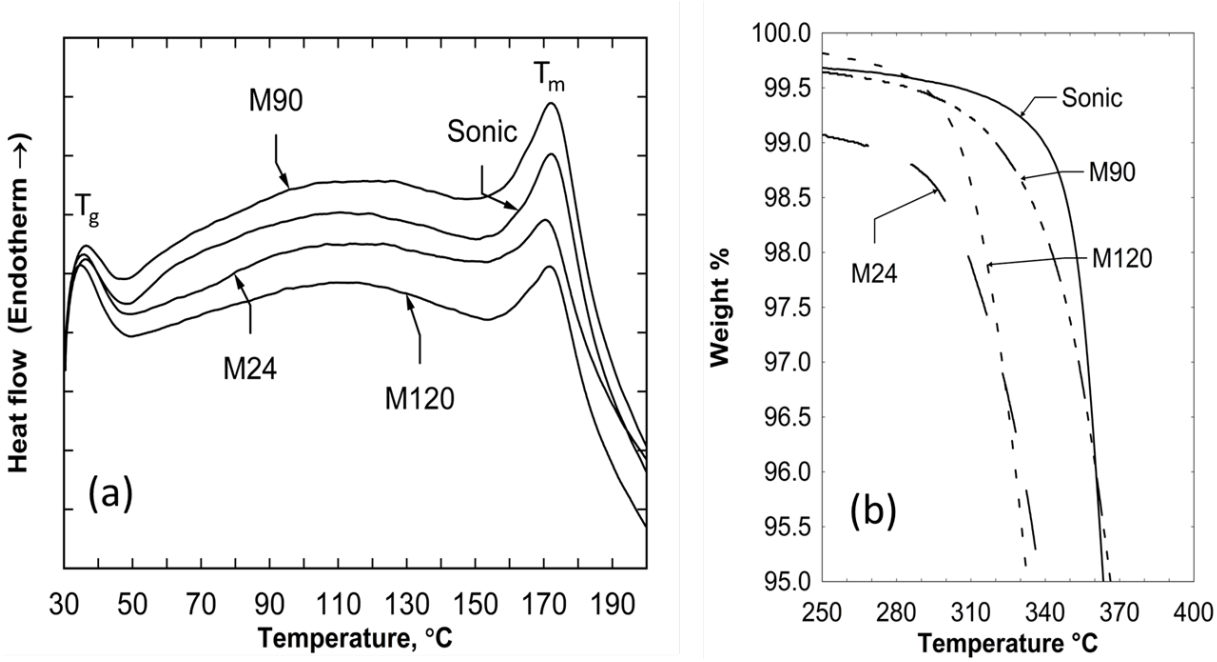

Figure 4. Heat flow differential scanning calorimetry (a) and weight loss thermogravimetric analysis (b) of membranes under nitrogen atmosphere and steady temperature increment of 10 °C/min

3.4. Mechanical strength and shrinkage

The tensile strength and elastic modulus for each membrane is given in Figure 5 as well as the areal shrinkage when the membranes were dried prior to the mechanical tests. The maximum tensile strengths at break were 1.51, 1.31, 1.26 and 1.47 MPa for M24, M90, M120 and Sonic respectively. These values were close to the 1.61 MPa maximum tensile strength value reported by Yu et al. [17] for their PVDF hollow fibre membranes. However, in the absence of a hydrophilic polymer such as the PVP used in this work, a much higher

maximum tensile strength of 4.5 MPa was reported by Lai et al. [12] for flat sheet PVDF membrane but at the cost of low water permeability. The high tensile strength of M24 seems to have been influenced by the membrane's very high shrinkage of about 50 %. The significant shrinkage of M24 is thought to be due to the limited unfolding or coupling of the polymer molecular chains as a consequence of the dope dissolution at the low temperature of 24 °C [1, 8, 9]. This proposal is apparently corroborated by the uniquely limited ductility of M24 in the stress-strain curves shown in Figure S.2. The other three membranes produced from dopes dissolved in higher energy environments showed shrinkage of ~10%. When M24 was annealed at 90 °C for 1 h before drying, however, the tensile strength and elastic modulus was found to have dropped significantly from 1.51 MPa to 0.90 MPa and from 10.4 MPa to 3.7 MPa, respectively. The areal shrinkage was found to decline correspondingly from 50% to 9%, clearly demonstrating that the high areal shrinkage of M24 is due to the low temperature of dope dissolution. Consequently, membranes produced at room temperature should be annealed at higher temperature if they are to be stored dried. Sonic with a tensile strength of 1.47 MPa and elastic modulus of 5.99 MPa is therefore seen to exhibit the highest load bearing capacity and stiffness for the stable membranes. The elastic modulus for M90 and M120 were 4.67 MPa and 4.42 MPa respectively. The mechanical strength results appear to follow the trend observed for the thermal stability tests with Sonic showing the highest thermal and mechanical stability and M24 (when the effect of shrinkage is excluded) showing the least.

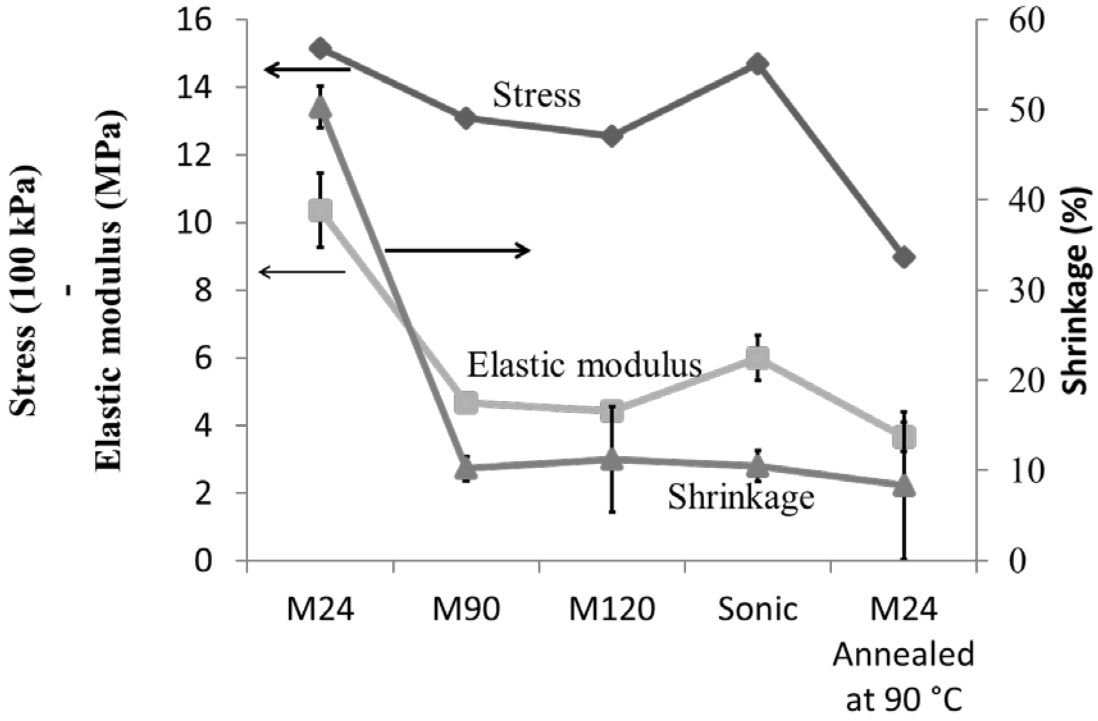

Figure 5. Mechanical strength and shrinkage property results. Error bars indicate computed standard error. Standard errors in the tensile stress values were <1%.

The shrinkage results presented in Figure 5 sheds some light on the observed relative membrane skin layer pores in the SEM images of Figure 2. Since M24 experienced a 50% areal shrinkage, it can be argued that the membranes pores observed in Figure 2 may be half of the actual pore areas for the wet membranes. Consequently, wet M24 may have similar pore sizes as M120.

3.5 Porosity

The membrane bulk porosity determined using Equation 2 is shown in Figure 6a. The porosity values obtained ranged from 86 to 90%. M24 had the highest bulk porosity of 90% while Sonic had the least bulk porosity of 86%. Consequently, dope sonication appears to result in less porous and dense membrane consistent with the SEM image of Figure 2. Although these values are very close, they seem to be important performance determinant as they appear to correspond with the trend of the membrane thermal and mechanical stability results discussed in Sections 3.3 and 3.4, respectively, as well as other performance parameter discussed in subsequent sections. The pore size distribution obtained by analysing

skin layer SEM surface images using ImageJ is shown in Figure 6b. Membrane pore size distribution determination from SEM images as performed in this work is a favoured technique for membrane pore analysis [30, 31]. Sonic shows an approximate bimodal normal pore size distribution while lognormal distribution better describes the pore size distribution for the other three membranes. UF membranes have been more commonly described by the lognormal distribution [31, 32] which further underscores the unique effect of dope sonication on membrane properties. The pores of dry Sonic are seen to range from about 2.5 nm to 25 nm with sharp cut-offs suggesting a relatively narrow pore distribution for the UF membrane. The other three membranes showed a large spread in pore sizes ranging from about 2.5 nm to about 80 nm indicating wider pore distribution UF membranes [33, 34]. Large pores contribute more to permeability but may result in reduced rejection [30, 31].

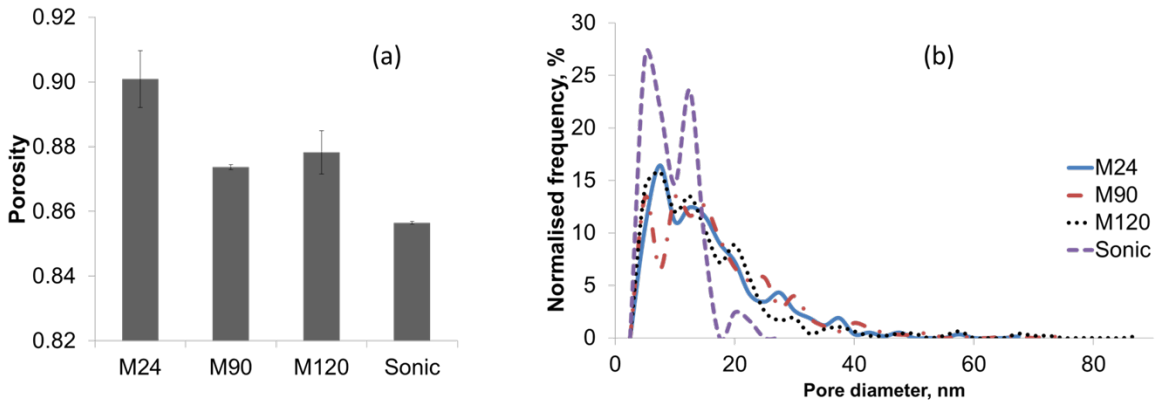

Figure 6. Membrane bulk porosity obtained gravimetrically (a) and pore size distribution on skin layer as obtained from image analysis of the SEM images of membrane selective surfaces (b). Error bars indicate computed standard error.

3.6. Wettability

The membrane wettability as measured by water CA is presented in Figure 7 showing that CAs for the membranes were between 76° and 95°. Images of typical water contact angles on the membranes are shown in Figure S.3. From Figure 7, M120 is seen to have the largest water CA of 95° while M90 had the lowest water CA of 76°. Although the difference between these results is significant with respect to the computed standard error, there appears to be no consistent pattern in the results. Considering that roughness (not quantified in this work) can greatly influence the outcome of water CA [35], the CA values for these

membrane may be said to be practically similar and thus not a strong function of dissolution condition. The water CA for PVDF membranes with added pore former has been reported variously as 74.4° [27], 82.9° [17], 76° and 93° [36]. This shows that the results of this study are within the expected range of previously reported wettability values for PVDF membranes.

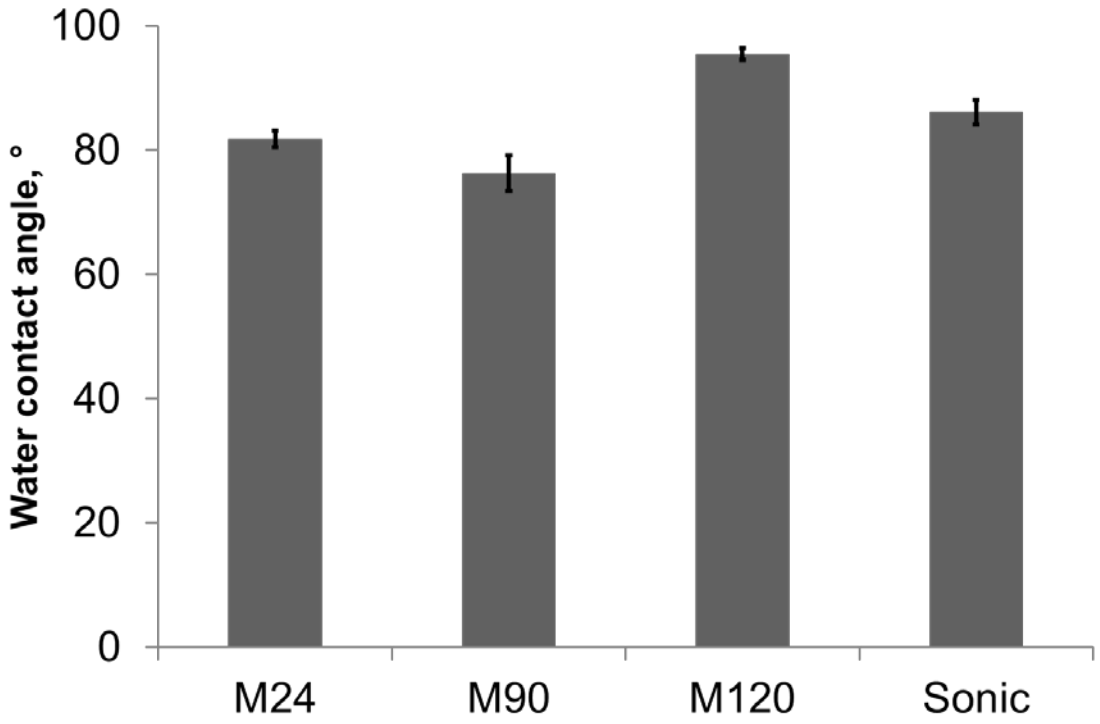

Figure 7. Membrane water contact angles measured using optical tensiometer operated at room temperature. Error bars indicate computed standard error.

3.7. Filtration performance

3.7.1 Flux and rejection

The membrane crossflow filtration performance at a TMP of 30 kPa is shown in Figure 8. The clean water flux results (Figure 8a) shows that very high J_0 of more than 600 $Lm^{-2}h^{-1}$ was obtained for M24 and M120. The similarity in J_0 for M24 and M120 strongly suggest similar skin layer pore sizes for the wet membranes as reasoned previously (Section 3.4).The lowest J_0 of about 180 $Lm^{-2}h^{-1}$ resulted for Sonic. The clean water flux results can be explained by the membrane porosity and surface pore size distribution shown in Figure 6. The larger surface pores and higher bulk porosity of M24, M90 and M120 allowed for higher permeation of water through the membrane while the denser morphology of small pores and

lower porosity means that only a relatively limited amount of water can be permeated through Sonic [30]. It may be noted that the clean water flux values observed in this work are significantly higher than the value of 5 $Lm^{-2}h^{-1}$ at a TMP of 175 kPa reported by Lai et al [12] for their PVDF membrane which was produced without the addition of a hydrophilic polymer such as the PVP used in this work. The addition of hydrophilic polymers to hydrophobic membrane materials is credited to increase hydrophilicity and pore formation [13, 37, 38].

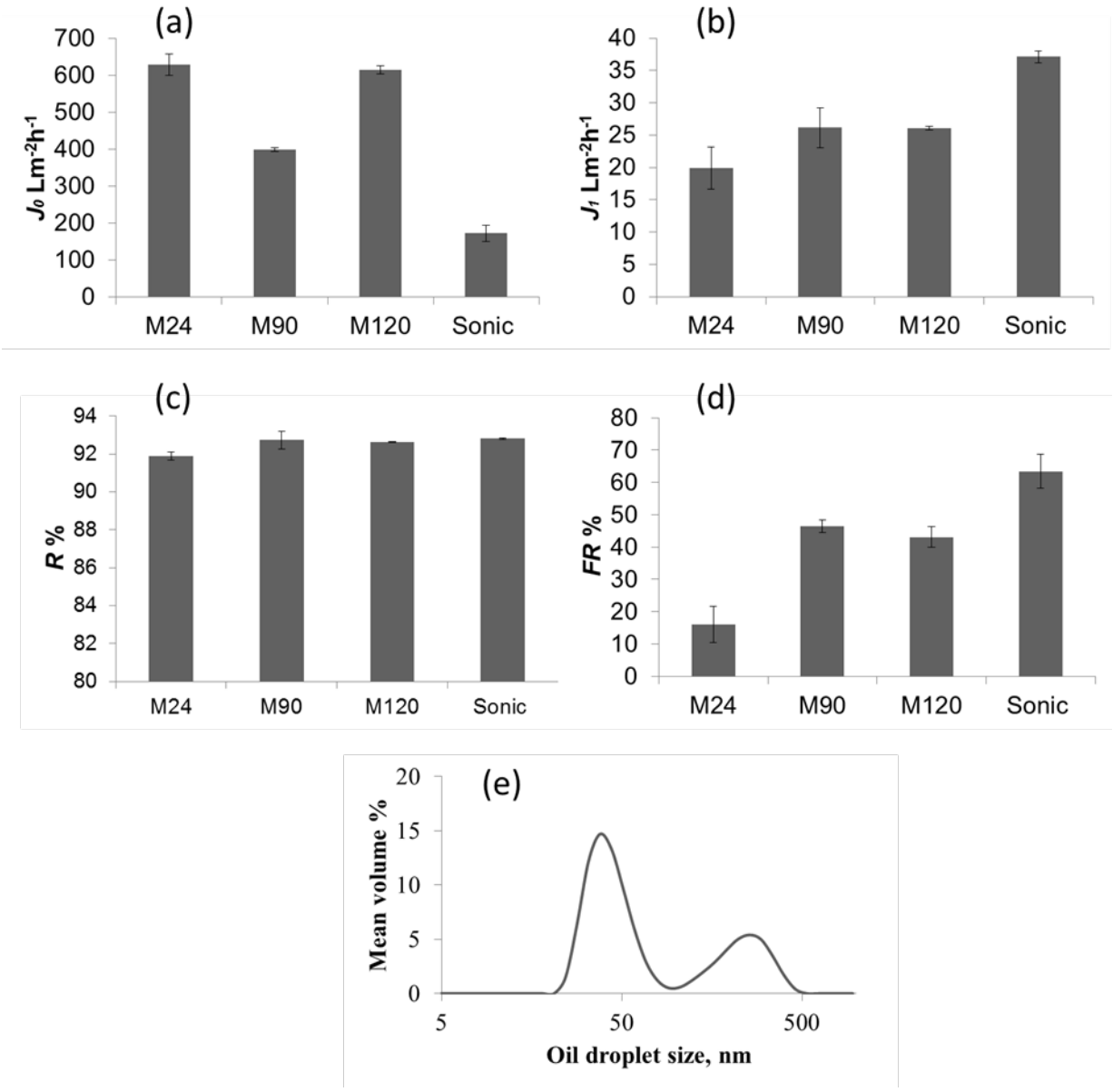

Figure 8. Membrane performance during crossflow clean water and oil emulsion filtration at TMP of 30 kPa. Clean water flux, J_0 (a), average permeate flux during oil emulsion filtration, J_1 (b), membrane TC rejections, R (c), membrane flux recovery after oil emulsion fouling and

cleaning with 0.1 M NaOH solutions, *FR* (d) and droplet size distribution for oil emulsion used as feed (e). Error bars indicate computed standard error.

The oil emulsion droplet sizes for the feed used to evaluate the fouling and rejection performance of the produced membranes ranged from 20 nm to 500 nm as shown in Figure 8e. Since the SEM observed pore sizes for the dry membranes are between 0 and 100 nm, it can be expected that both pore blocking and cake formation are possible fouling mechanism for the filtration systems [39]. The average permeate flux during the oil emulsion filtration, J_1, is shown in Figure 8b. The sample trend is an almost reversal of J_0 with the Sonic showing the highest flux value of 37 $Lm^{-2}h^{-1}$ while M24 had the lowest flux of 20 $Lm^{-2}h^{-1}$. The J_1 for M90 and M120 were both approx. 26 $Lm^{-2}h^{-1}$. The rejection of TC by the membranes during the oil emulsion filtration is shown in Figure 8c. It can be seen that the rejection value for all the membranes are similar at a value of 92% despite the lower pore size observed for the Sonic. An explanation for the rejection results may be advanced along the line that the larger pores in M24, M90 and M120 were rapidly blocked by foulants thereby giving the effect of similar TC rejection. If this reasoning is correct, it is expected that Sonic will have the better *FR*. The *FR*, after oil emulsion fouling and cleaning with a 0.1 M NaOH solution for the membranes, is shown in Figure 8d. As expected, Sonic exhibited the best *FR* of 63% while M24 had the lowest *FR* of 26%. The *FR* for M90 and M120 were 46% and 43% respectively. Overall, the Sonic can be said to be suitable for the filtration of more challenging feed while the stable M120 with high J_0 is more suitable for the high flux filtration of low fouling feeds.

Although high permeate flux under severe fouling conditions and enhanced flux recovery is often associated with hydrophilicity improvement [40], membrane wettability differences cannot explain the flux results obtained in this work since the average CA for Sonic with the best flux recovery was 86° while M24 with the lowest flux recovery had a slightly lower water CA of 82°. The wettability values are practically alike as discussed earlier but a lower CA for Sonic would have been expected to explain the filtration results obtained. As pointed out earlier, a consideration of the skin layer pore size distributions for the membranes (Figure 6b) may suggest that Sonic with lower pore sizes and narrow pore size distribution should provide better rejection [30, 31]. But as that was not the case (Figure 8c), a reasonable explanation of the filtration results will emphasise the role of skin layer pore size where larger pores were extensively and rapidly blocked [39, 41] and de-emphasise the influence of

surface hydrophilicity. Although the deformable property of oil droplets have been reported to allow the squeezing of large droplet particles into much smaller membrane pores at operating pressure of 150 kPa [42], the low TMP value of 30 kPa used in this work is thought to be insufficient to cause significant oil droplet deformation so that only large pores were effectively blocked. The implication here would be that Sonic with smaller pores will experience more cake fouling and limited pore blocking [39]. The proposed rapid pore blocking for M24, M90 and M120 due to their larger pore sizes also explain their observed lower J_1. This can be seen by considering that a significant amount of the pores in these membranes are greater than the minimum oil droplet size of 20 nm while only a small fraction of the pores in Sonic have sizes greater than 20 nm. Consequently, the rapid blockage of large pores would affect the J_1 more for M24, M90 and M120 compared to Sonic. The limited *RF* for M24, M90 and M120 relative to Sonic is also consistent with this explanation in which pore blocking increased the problem of irreversible fouling [43]. It may therefore be concluded that the narrow pore diameter range (<25 nm) for Sonic allowed for adequate percolation of water molecules but was less accessible to the oil droplets (>20 nm) in the emulsion resulting in sustained high water permeation and low pore blocking as oil droplets were substantially excluded from the membrane pores.

In addition, the relatively smooth surface for Sonic with limited surface depressions as was shown in the SEM images of Figure 2 may have contributed significantly to its better flux recovery as foulants are less likely attached onto a smooth surface when compared to a rough surface [44].

3.7.2 Cake formation and modelling

After the filtration tests, significant differences in the membranes were clearly seen upon visual inspection. Images of representative fouled membranes after cleaning are shown in Figure 9. The Sonic showed the most colouring followed by M24 while M120 seems to show the least colouring. The more intense yellowish colouring of Sonic may be indicative of more surface or cake fouling. The intense surface colouring on Sonic is expected since with smaller pores and higher permeate flux during the oil emulsion filtration, more rejected foulant may deposit on the membrane surface as cake. Surprisingly, the instantaneous J_1 taken at the 2 h mark (Figure 10a) shows that despite the more intense surface colouring indicative of more surface fouling, Sonic sustained not only a higher overall J_1, but also maintained higher permeate flux to the last moment of the fouling test.

Figure 9. Image of representative membranes after fouling and cleaning with 0.1 M NaOH, from left to right M24, M90, M120 and Sonic

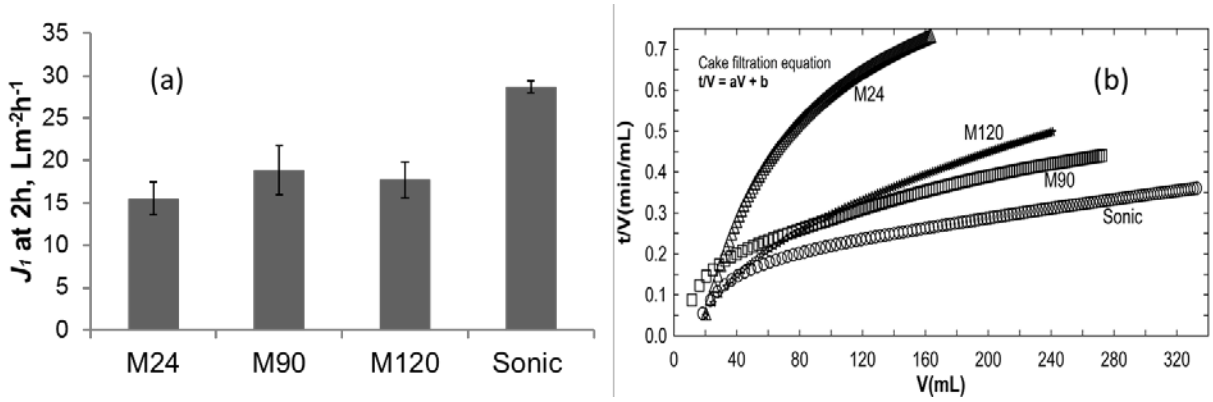

Figure 10. Permeate flux during filtration of oil emulsion at 2 h (a), cake filtration model plots (b). Error bars indicate computed standard error.

To elucidate the fouling mechanism responsible for the varied colouring of the membranes and their filtration behaviour, simple filtration modelling was employed. A linear relation when filtration-time/filtrate-volume (t/v) is plotted against filtrate-volume (v) has been shown to be indicative of cake fouling [39, 41, 45]. These plots are presented in Figure 10b. The four membranes show an early non-linear trend which is indicative of pore blocking [39, 41, 43, 45]. The non-linear trend was continued for almost the entire filtration volume for M24 suggestive of minimal cake fouling but extensive pore blocking. That M24 had the lowest J_1

supports the claim that the principal fouling for this membrane was pore blocking. However, it has to be considered that some amount of cake deposition did occur on M24 after the pores were sufficiently blocked giving rise to the observed colouring. The limited colouring of M120 may be due to its limited permeate volume when compared to M90 and Sonic (Figure 10b). In addition, M120 showed the highest polar *F(β)* (Figure 3) which is likely to reduce its attachment to the non-polar oil droplets [8]. In the same vein, M24 with the least *F(β)* is expected to show greater affinity to the non-polar oil.

The initial non-linear trend for Sonic in Figure 10b was seen to give way after only a small filtration volume to an extended linear relationship indicative of extensive cake fouling which is consistent with the cake fouling mechanism advanced in this work for this membrane. The filtration experiment in this work is set up such that the concentration of the feed increased as permeate is removed (see Figure 1). As shown in Figure 10b, for the 2 h duration of the filtration test, more permeate volume was removed from the feed by Sonic than the other membranes implying that the former was charged with more concentrated feed towards the end of the 2 h filtration tests. This fact is probably partly responsible for the increased surface colouring observed for this membrane arising from increased cake deposition due to higher feed concentration. It is interesting that despite the significant surface colouring indicative of more cake formation and the more concentrated feed towards the end of the filtration, Sonic retained the highest J_1 at 2 h (Figure 10a) which highlights its superior filtration performance. It is also important to note that no deviation from a straight line was observed for any of the membrane towards the end of the filtration period which suggests that cake compression was minimal or absent [45]. This observation corroborate the earlier proposal that although oil droplets are deformable and can penetrate much smaller pores than their diameters, the TMP of 30 kPa at which the experiment in this work were perform was probably too low for such deformation to occur so that only pores bigger than the oil droplets were blocked.

3.7.3. Porosity correlations

The results presented so far highlight major differences in membrane properties and performance as a result of altering the conditions of the dope dissolution. To more fully comprehend the basis for the changes in performance and properties, the results were analysed more closely to determine whether there is a primary parameter directly altered by the dissolution conditions and which then impacted other membrane properties. An overview of the performance evaluations conducted seems to suggest a consistent pattern in which M24

and Sonic appear to occupy opposite extremes while M90 and M120 take the middle place following approximately the bulk porosity trend of Figure 6b. To quantify this apparent relationship, linear regressions of the performance data against the bulk porosity were made and presented in Figure 11.

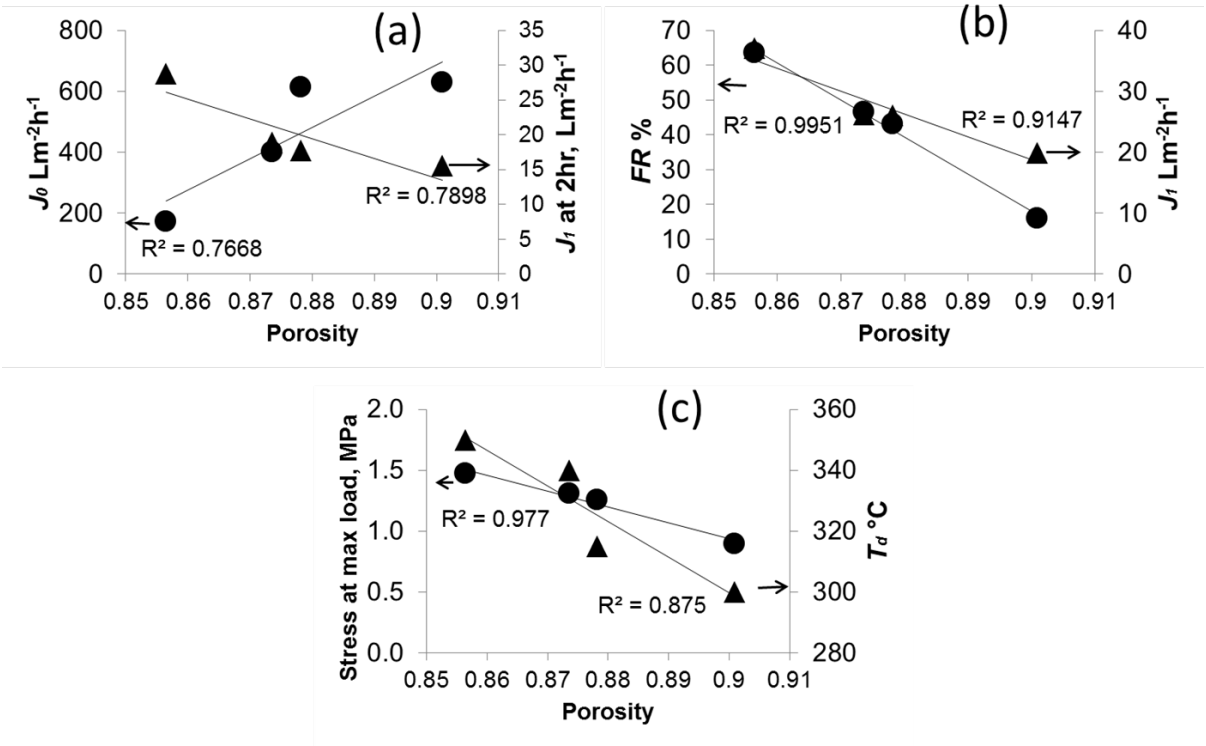

Figure 11. Membranes performance correlations to bulk porosity for water flux, J_0, and emulsion permeate flux at 2 h, J_1 (a) flux recovery, *RF*, and average emulsion permeate flux, J_1 (b) tensile stress at maximum load and temperature for the onset of thermal degradation T_d (c).

Interestingly, all the performance data show reasonable to strong correlations to the bulk porosity as measured by the linear regression coefficient (R^2). The minimum R^2 observed was for J_0 which however was a reasonable R^2 of 0.7668, while the largest R^2 was for mechanical strength which showed strong correlation of 0.9951. A schematic elucidation of how porosity/pore size can influence such varying key membrane performance parameters is presented in Figure 12. Figure 12 assumes that the pore distribution, pore shape and number of pores for the membranes are alike. The probable implications are that membrane porosity/pore size is an important tool for the design of membrane for specific applications

and that such tailored design can be achieved by simply altering the condition of the initial PVDF polymer dissolution.

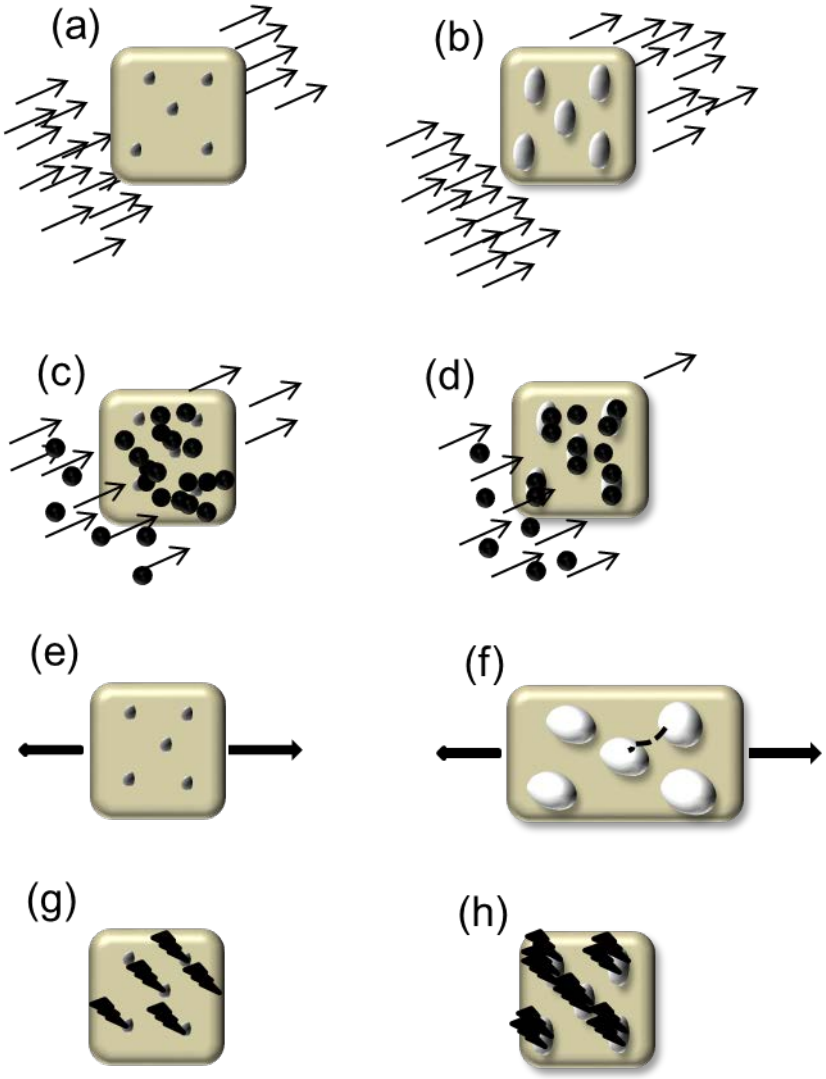

Figure 12. Schematic elucidation of porosity/pore size influence on key membrane performance parameters assuming similar number of pores. Low water flux – small flow area (Poiseuille's Law) [46] (a); high water flux – large flow area (Poiseuille's Law) [46] (b); good emulsion permeation/flux recovery – less pore blocking and more cake deposition [39, 41, 43] (c); poor emulsion permeation/flux recovery – extensive pore blocking and limited cake deposition [39, 41] (d); good mechanical stability – more membrane material supporting load (less effective stress) [47] (e); poor mechanical stability – less load bearing material (more effective stress) [47] (f); good thermal stability – limited thermal attack fronts or end chains [25] (g); poor thermal stability – large area for thermal attack or end chains [25] (h).

3.7.4. Dope dissolution environment

Previous studies on the effects of physical dissolution conditions on the properties of PVDF membranes have focused exclusively on temperature which results in gradual and predictable changes in the properties of the synthesised membrane [1, 7, 8]. The properties of the Sonic membrane in this work is starkly different from the other membranes suggesting that a mere temperature effect cannot explain the unique properties. Since several physical mechanisms develop from ultrasonication such as heating, structural effects, compression and rarefaction, turbulence and cavitation [10, 15], it appears that the unique properties of the Sonic membrane is due to the combined effects of several physical processes. These physical processes can be simply referred to as providing a more energetic dissolution environment.

The observed effects of dissolution environments in terms of their energy level can be related to the degree of unfolding of the polymer molecular chains and their entanglements following Wang et al. [1]. As discussed in earlier sections, the energy of the PVDF dissolution environment defines to what extent the polymer molecular chains can unfold/dissolve and to what extent the unfolded chains are entangled or resist gelation [1, 7, 8]. In a low temperature environment, the chains are folded [1, 8] or partially dissolved even though visually clear [7, 8] and therefore achieve limited permanent entanglement resulting in an unstable polymer framework. This is observed as the large shrinkage of M24 upon drying highlighting that its loose framework allowed for the presence of significant amount of water and when the embedded water was dried out, the membrane structure was too weak to maintain its original volume and therefore collapsed. However, as the temperature of dope dissolution increased, the kinetic energy of the polymer allowed for greater unfolding and therefore greater entanglement [1] resulting in a permanent structure when the membrane was dried of water. The highly energised environment provided by ultrasonication resulted in significant unfolding of the polymer chains and their extensive entanglement. The extensive entanglement is hypothesised to cause a permanent grid system with uniform pores of small size and enhanced mechanical properties. Consequently, dope sonication provides a unique technique to achieve comparatively small pore size membrane with narrow pore size distribution and strong physical properties. A conceptualisation of the effects of different dope dissolving conditions on PVDF polymer networks as wet and dry membranes following Wang et al. [1] is shown in Figure 13.

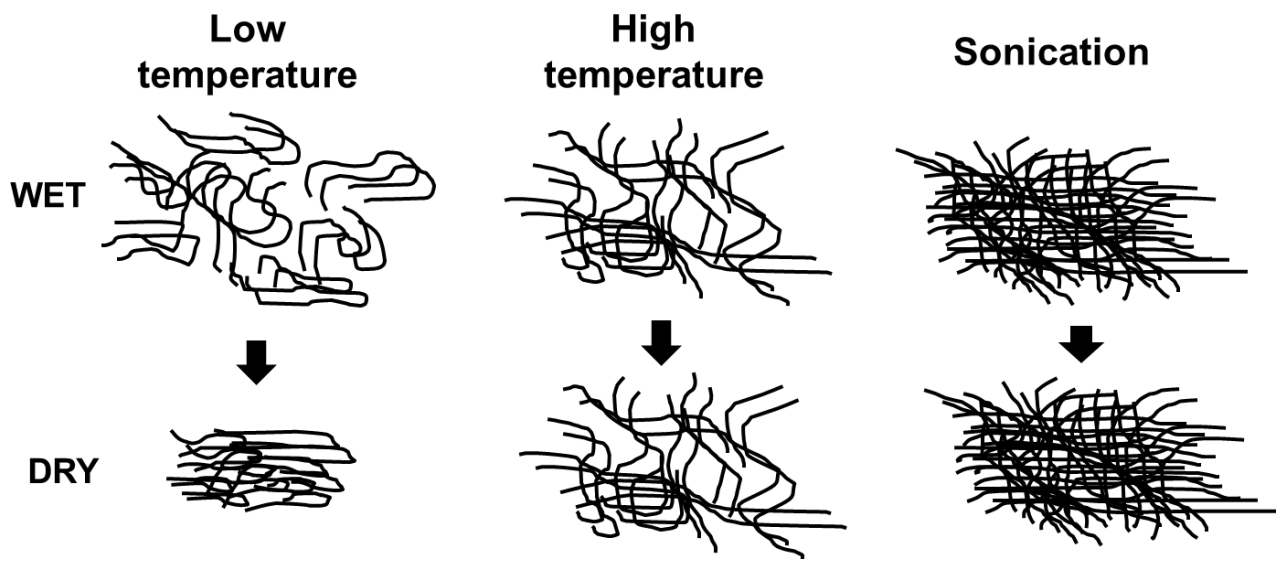

Figure 13. Schematic representation of the effects of different dope dissolving conditions on PVDF polymer networks entanglement [1] as wet and dry membranes.

4. Conclusion

This study contributes to a growing body of research that demonstrates the important effects of PVDF dissolution conditions on the properties of the membranes. It is shown that not only the specific temperature of dope dissolution but other physical forms of energy inputs such as are generated via ultrasonication have significant effects on the performance of UF membranes and therefore may be employed for specific membrane design. Dope dissolved by ultrasonication was shown to result in a membrane with dense structure and reduced porosity, narrow size distribution of small pores and reasonably smooth skin layer relative to the other membranes produced under identical conditions excepting the polymer dissolution process. Even though this membrane suffered from reduced clean water flux when compared to the other membranes produced without sonication, its unique properties were shown to result in enhanced thermal stability, improved mechanical strength and outstanding oil emulsion filtration performance of high permeate flux and high *RF*. Consequently, Sonic may be suitable for filtration under more practical conditions of challenging feed while the high clean water flux of M120 may allow for high productivity under less challenging conditions. The performances of the membranes evaluated in this work irrespective of the mode of original polymer dissolution showed strong correlations to the membrane porosity suggesting a possible convenient means for UF membrane design achievable by simply altering the mode

of polymer dissolution. The observed difference in the properties of membranes due to dope dissolution in different energy environment was related to the degree of unfolding/dissolution of the polymer molecular chains and their entanglements.

5. Acknowledgement

The financial support provided by Victoria University to Ikechukwu A. Ike through the Victoria University International Postgraduate Research Scholarship is gratefully acknowledged. Sincere gratitude to Ludovic F. Dumée, Deakin University, for his many insightful suggestions and for acquiring the SEM cross section images. Anbharasi Vanangamudi, Victoria University, is also gratefully acknowledged for acquiring the surface SEM images.

References

[1] X. Wang, X. Wang, L. Zhang, Q. An, H. Chen, Morphology and Formation Mechanism of Poly(Vinylidene Fluoride) Membranes Prepared with Immerse Precipitation: Effect of Dissolving Temperature, Journal of Macromolecular Science, Part B, 48 (2009) 696-709.
[2] F. Liu, N.A. Hashim, Y. Liu, M.R.M. Abed, K. Li, Progress in the production and modification of PVDF membranes, Journal of Membrane Science, 375 (2011) 1-27.
[3] G.-d. Kang, Y.-m. Cao, Application and modification of poly(vinylidene fluoride) (PVDF) membranes – A review, Journal of Membrane Science, 463 (2014) 145-165.
[4] B. Wu, K. Li, W.K. Teo, Preparation and characterization of poly(vinylidene fluoride) hollow fiber membranes for vacuum membrane distillation, Journal of Applied Polymer Science, 106 (2007) 1482-1495.
[5] A. Bottino, G. Camera-Roda, G. Capannelli, S. Munari, The formation of microporous polyvinylidene difluoride membrane by phase separation, Journal of Membrane Science, 57 (1991) 1-20.
[6] A. Gugliuzza, E. Drioli, New performance of hydrophobic fluorinated porous membranes exhibiting particulate-like morphology, Desalination 240 (2009) 14 - 20.
[7] D.-J. Lin, K. Beltsios, T.-H. Young, Y.-S. Jeng, L.-P. Cheng, Strong effect of precursor preparation on the morphology of semicrystalline phase inversion poly(vinylidene fluoride) membranes, Journal of Membrane Science, 274 (2006) 64-72.
[8] A.L. Ahmad, N. Ideris, B.S. Ooi, S.C. Low, A. Ismail, Morphology and polymorph study of a polyvinylidene fluoride (PVDF) membrane for protein binding: Effect of the dissolving temperature, Desalination, 278 (2011) 318-324.
[9] M. Li, I. Katsouras, C. Piliego, G. Glasser, I. Lieberwirth, P.W.M. Blom, D.M. de Leeuw, Controlling the microstructure of poly(vinylidenefluoride) (PVDF) thin films for microelectronics, Journal Material Chemistry C, 1 (2013) 7695–7702.
[10] I. Masselin, X. Chasseray, L. Durand-Bourlier, J.-M. Lainé, P.-Y. Syzaret, D. Lemordant, Effect of sonication on polymeric membranes, Journal of Membrane Science, (2001) 213-220.
[11] A. Bottino, G. Capannelli, A. Comite, Preparation and characterization of novel porous PVDF-ZrO2 composite membranes, Desalination, 146 (2002) 35-40.

[12] C.Y. Lai, A. Groth, S. Gray, M. Duke, Preparation and characterization of poly(vinylidene fluoride)/nanoclay nanocomposite flat sheet membranes for abrasion resistance, Water Research, 57 (2014) 56-66.
[13] H. Rajabi, N. Ghaemi, S.S. Madaeni, P. Daraei, M.A. Khadivi, M. Falsafi, Nanoclay embedded mixed matrix PVDF nanocomposite membrane: Preparation, characterization and biofouling resistance, Applied Surface Science, 313 (2014) 207-214.
[14] S. Liang, K. Xiao, Y. Mo, X. Huang, A novel ZnO nanoparticle blended polyvinylidene fluoride membrane for anti-irreversible fouling, Journal of Membrane Science, 394-395 (2012) 184-192.
[15] B. Banerjee, Recent developments on ultrasound assisted catalyst-free organic synthesis, Ultrasonics sonochemistry, 35 (2017) 1-14.
[16] B. Mohammadi, A.A. Yousefi, S.M. Bellah, Effect of tensile strain rate and elongation on crystalline structure and piezoelectric properties of PVDF thin films, Polymer Testing, 26 (2007) 42-50.
[17] L.-Y. Yu, Z.-L. Xu, H.-M. Shen, H. Yang, Preparation and characterization of PVDF–SiO2 composite hollow fiber UF membrane by sol–gel method, Journal of Membrane Science, 337 (2009) 257-265.
[18] J.-F. Li, Z.-L. Xu, H. Yang, Microporous polyethersulfone membranes prepared under the combined precipitation conditions with non-solvent additives, Polymers for Advanced Technologies, 19 (2008) 251-257.
[19] L. Priya, J.P. Jog, Polymorphism in Intercalated Poly(vinylidene fluoride)/Clay Nanocomposites, Journal of Applied Polymer Science, 89 (2003) 2036–2040.
[20] C.Y. Lai, A. Groth, S. Gray, M. Duke, Enhanced abrasion resistant PVDF/nanoclay hollow fibre composite membranes for water treatment, Journal of Membrane Science, 449 (2014) 146-157.
[21] D.R. Dillon, K.K. Tenneti, C.Y. Li, F.K. Ko, I. Sics, B.S. Hsiao, On the structure and morphology of polyvinylidene fluoride–nanoclay nanocomposites, Polymer, 47 (2006) 1678-1688.
[22] D. Shah, P. Maiti, E. Gunn, D.F. Schmidt, D.D. Jiang, C.A. Batt, E.P. Giannelis, Dramatic enhancements in toughness of Polyvinylidene fluoride nanocomposites via nanoclay directed crystal structure and morphology, Advanced Materials, 16 (2004) 1173-1177.
[23] R.M. Cornell, U. Schwertmann, The Iron Oxides: Structures, Properties, Reactions, Occurences and Uses, 2nd Edition ed., WILEY-VCH Verlag GmbH & Co. KGaA, Weinheim, 2003.
[24] M.D. Lekgoathi, L.D. Kock, Effect of short and long range order on crystal structure interpretation: Raman and powder X-ray diffraction of LiPF(6), Spectrochimica acta. Part A, Molecular and biomolecular spectroscopy, 153 (2016) 651-654.
[25] C.L. Beyler, M.M. Hirschler, Thermal Decomposition of Polymers, in: P.J. DiNenno (Ed.) SFPE Handbook of Fire Protection Engineering National Fire Protection Association, 2002.
[26] Solvay, Solef PVDF Design & Processing Guide, in, Solvay Specialty Polymers, 2015.
[27] Y. Zhang, J. Zhao, H. Chu, X. Zhou, Y. Wei, Effect of modified attapulgite addition on the performance of a PVDF ultrafiltration membrane, Desalination, 344 (2014) 71-78.
[28] A. Karatrantos, N. Clarke, R.J. Composto, K.I. Winey, Entanglements in polymer nanocomposites containing spherical nanoparticles, Soft Matter, 12 (2016) 2567--2574.
[29] R. Mangal, S. Srivastava, L.A. Archer, Phase stability and dynamics of entangled polymer-nanoparticle composites, Nature communications, 6 (2015) 7198.
[30] S. Mochizuki, A.L. Zydney, Theoretical analysis of pore size distribution effects on membrane transport, Journal of Membrane Science, 82 (1993) 211-227.
[31] S.R. Wickramasinghe, S.E. Bower, Z. Chen, A. Mukherjee, S.M. Husson, Relating the pore size distribution of ultrafiltration membranes to dextran rejection, Journal of Membrane Science, 340 (2009) 1-8.
[32] W.R. Bowen, J.S. Welfoot, Modelling of membrane nanofiltration—pore size distribution effects, Chemical Engineering Science, (2002) 1393–1407.
[33] C. Binnie, M. Kimber, Basic Water Treatment, in, ICE Publishing, London, 2013.
[34] A. Cipollina, G. Micale, L. Rizzuti, Seawater desalination, in: Green Energy and Technology, Spinger-Verlag, Heidelberg, 2009.

[35] D.J. Shaw, Introduction to colloid and surface chemistry, Butterworth & Co. (Publishers) Ltd, London, 1980.
[36] E. Fontananova, J.C. Jansen, A. Cristiano, E. Curcio, E. Drioli, Effect of additives in the casting solution on the formation of PVDF membranes, Desalination, 192 (2006) 190-197.
[37] A. Pagidi, R. Saranya, G. Arthanareeswaran, A.F. Ismail, T. Matsuura, Enhanced oil–water separation using polysulfone membranes modified with polymeric additives, Desalination, 344 (2014) 280-288.
[38] H. Basri, A.F. Ismail, M. Aziz, Polyethersulfone (PES)–silver composite UF membrane: Effect of silver loading and PVP molecular weight on membrane morphology and antibacterial activity, Desalination, 273 (2011) 72-80.
[39] T. Mohammadi, A. Kohpeyma, M. Sadrzadeh, Mathematical modeling of flux decline in ultrafiltration, Desalination, 184 (2005) 367-375.
[40] L. Yan, S. Hong, M.L. Li, Y.S. Li, Application of the Al2O3–PVDF nanocomposite tubular ultrafiltration (UF) membrane for oily wastewater treatment and its antifouling research, Separation and Purification Technology, 66 (2009) 347-352.
[41] Y. Ye, P. Le Clech, V. Chen, A.G. Fane, B. Jefferson, Fouling mechanisms of alginate solutions as model extracellular polymeric substances, Desalination, 175 (2005) 7-20.
[42] A. Hong, A.G. Fane, R. Burford, Factors affecting membrane coalescence of stable oil-in-water emulsions, Journal of Membrane Science, 222 (2003) 19-39.
[43] L. De Angelis, M.M.F. de Cortalezzi, Ceramic membrane filtration of organic compounds: Effect of concentration, pH, and mixtures interactions on fouling, Separation and Purification Technology, 118 (2013) 762-775.
[44] X. Cao, J. Ma, X. Shi, Z. Ren, Effect of TiO2 nanoparticle size on the performance of PVDF membrane, Applied Surface Science, 253 (2006) 2003-2010.
[45] H.T. Madsen, Membrane Filtration in Water Treatment – Removal of Micropollutants, in: Chemistry of Advanced Environmental Purification Processes of Water, Elsevier B.V., 2014, pp. 199-248.
[46] R.W. Baker, Membrane technology and applications, 3 ed., John Wiley & Sons, United Kingdom, 2012.
[47] P. Ghavami, Stress and strain, in: P. Ghavami (Ed.) Mechanics of Materials, Springer International Publishing, Switzerland, 2015, pp. 143-162.